Heavy snowfall event over the Swiss Alps: Did wind shear impact secondary ice production?

Zane Dedekind[*1], Jacopo Grazioli[*2], Philip H. Austin[1], and Ulrike Lohmann[3]

[1]Department of Earth, Ocean, and Atmospheric Sciences, University of British Columbia, Earth Sciences Building, 2207 Main Mall, Vancouver, BC, V6T 1Z4, Canada
[2]Environmental Remote Sensing Laboratory (LTE), École Polytechnique Fédérale de Lausanne (EPFL), Lausanne, Switzerland
[3]Institute of Atmospheric and Climate Science, ETH Zurich, Switzerland
[*]Equally contributing authors

We sincerely thank Reviewer 2 for the constructive feedback. The suggestions and comments considerably improved the quality of the manuscript.

Below we present a detailed response with the reviewer comments in black, our responses in blue and additions to the manuscript in blue italics.

Specific comments

1. It was difficult follow the entire manuscript, probably because of a lack of descriptions of model simulations (or I cannot find at least). The authors should give detailed, careful explanations of simulations for people who do not have model background. Specifically, I have the following questions:

   – For Eqs. 1-3, what does "BR" stand for? What do BR28, BR2.8T, and BR-Sot mean? Because I could not know them, understanding the following descriptions was very difficult for me.

   Indeed, we did not specifically mention what BR mean. BR refers to breakup. We also added which parameterization is associated with its reference:

   In this study of the heavy snowfall event during which high K_{dp} values were recorded, we use the parameterizations for ice-graupel collisional breakup (BR) from Dedekind et al. (2021, BR28 and BR2.8T) and Sotiropoulou et al. (2021, BR-Sot) in COSMO in different forms.

   References to the simulations were given beneath the equations and their descriptions. However, we now provide some more context to the description.

   Because of an inconsistency between the hail particles and their corresponding fall velocity used in Takahashi et al. (1995), which is described in more detail in Dedekind et al. (2021), all the parameterizations (Eqs. 4, 5 and 6) have scaling factors. Equations 4 and 5 were applied in Dedekind et al. (2021) for the BR28 and BR2.8T simulations

respectively. The BR28 simulation is scaled by α=10 and has a slower decay rate of fragment number at warmer temperatures represented by γ_{BR}=2.5 and equation 5 is scaled by 100 while using the same decay rate of fragment numbers of γ_{BR}=5 as used in Sullivan et al. (2018) which was derived from Takahashi et al. (1995). Equation 6, for the BR-Sot simulation, was applied in Sotiropoulou et al. (2021). They used a scaling parameter, $\bar{D}/\bar{D}_0$, that was applied to the breakup parameterization from Sullivan et al. (2018) where $\bar{D}_0$ = 0.02 mm.

– What does N_BR mean?

$\aleph_{BR}$ is the number of fragments generated per collision given all the parameters in Eqs. 4, 5 and 6. We added this to the description of the equations.

– Lines 164-165: To me this sentence does not make sense at all. Need detailed explanations. What is scaled; what are BR, Sot, 2.8T?

Thank you, we added more detail to the description of the equations as described above.

– What is RS simulation? I could not easily find the description about the simulation.

We added more information to the text to make it clear.

Simulations were conducted including several SIP processes, which consisted of ice-graupel collisions (as thoroughly discussed in section 2.2.2 below) and a control simulation, referred to as the rime splintering (RS) simulation, where only rime splintering was active as a SIP process.

– It seems to me that the radar reflectivity from the simulations is very large. For many regions below 5-6 km, reflectivity attained or exceeded 30 dBZ for all simulations. The authors mentioned the size of simulated particles, but still I think too large for snow scattering at X-band, otherwise it was graupel. Was graupel produced in the entire cloud below 5 km? Please give detailed settings of calculation of reflectivity from the simulation data.

1) During the duration of the simulations, all simulations produced graupel, albeit at lower mass concentrations for the collisional breakup simulations (Fig. 5). There is a strong correlation between the graupel concentration and the reflectivity which is most likely the dominant factor in the overall calculation of reflectivity (Fig. 5a). 2) Rime splintering was very low, which is typical for wintertime MPCs (Fig. 7f here and e.g., Henneberg et al., 2017; Dedekind et al., 2021), the ice and snow crystals grew mainly by depositional growth and aggregation to much larger sizes compared to the collisional breakup simulations (Fig. 6c). The snow crystals, especially, were twice the size of those in the breakup simulations (Fig. 6b, over 2 mm in diameter). Below we show Hovmöller plots (Figs. 1 and 2) for the size diameters for ice crystals, snow, and graupel from 15:00 to 17:30 UTC showing that the snow and graupel particles reached diameters of over 5.1 mm and 8 mm, respectively. 3) The rain mass and number concentrations were also substantially higher in the rime splintering simulation. All these factors may have contributed to the large overestimation of Z_H apart from the issues that arise from size sorting which is discussed in the manuscript. We added a similar description to Section 3.2.1.

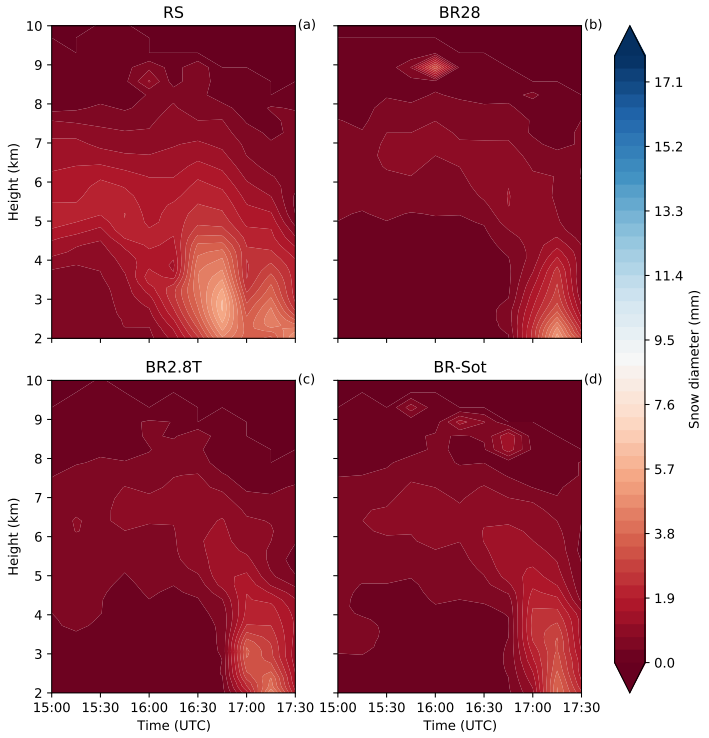

Figure 1. Hovmöller diagrams of snow diameters for panels **(a)** RS , **(b)** BR28, **(c)** BR2.8T and **(d)** BR-Sot between 15:00 and 17:30 UTC.

Here we briefly show the calculation of the simulated Z_{H} (Appendix B, Seifert, 2002). Calculating Z_{H} from the two-moment cloud microphysics scheme would not be possible without approximations and assumptions. The following relationship for the radar reflectivity of drops (Z_{w}), using the Rayleigh approximation for the cross-section of drops (Eq. 1), results in:

$$\eta_w = \frac{\pi^5 |K_w|^2}{\lambda_R^4} \int_0^\infty D^6 f_w(D) dD \tag{1}$$

where D is the particle diameter, λ_R is the wavelength of radar radiation, η_w is the volumetric liquid water content, $f_w(D)$ is the number density distribution function for liquid water and K_w^2= 0.93 the dielectric constant of liquid water. The reflectivity factor for cloud water is given by:

$$\tilde{Z}_w = \frac{\lambda_R^4}{\pi^5 |K_w|^2} \eta_w = \int_0^\infty D^6 f_w(D) dD = \left(\frac{6}{\pi \rho_w}\right)^2 \int_0^\infty x^2 f_w(x) dx = \left(\frac{6}{\pi \rho_w}\right)^2 Z_w \tag{2}$$

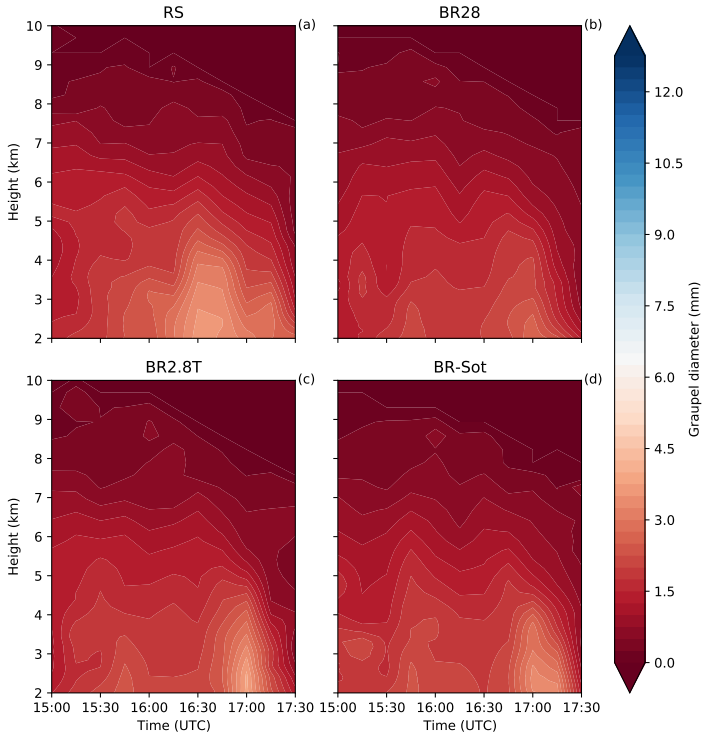

Figure 2. The same as Figure 1, but for graupel.

where ρ_w is the water density. Because of the backscatter behavior for the mass-equivalent diameter with regards to ρ_w and ρ_i (ice density), the same applies to graupel, which is described as a spherical ice particle

$$\eta_g = \frac{\pi^5 |K_i|^2}{\lambda_R^4} \left(\frac{6}{\pi \rho_i} \right)^2 \int_0^\infty x^2 f_g(x) dx_1 \tag{3}$$

where x is the particle mass, $f_g(x)$ is the number density distribution function for graupel and K_i^2= 0.176 is the dielectric constant of ice. The radar reflectivity factor for ice particles (e.g., graupel) is given by:

$$\tilde{Z}_g = \frac{\lambda_R^4}{\pi^5 |K_w|^2} \eta_g = \frac{|K_i|^2}{|K_w|^2} \left(\frac{6}{\pi \rho_i} \right)^2 \int_0^\infty x^2 f_g(x) dx = \frac{|K_i|^2}{|K_w|^2} \left(\frac{6}{\pi \rho_i} \right)^2 Z_g. \tag{4}$$

For melting ice particles, however, K_w must be used instead of K_i. In our study, the surface and in-situ cloud temperatures were below 0 °C. Therefore, more information on the reflectivity calculations for melting ice particles can be found in Seifert (Appendix B, 2002). Finally, the radar reflectivity factor is given by:

$$dBZ = \frac{10}{\ln 10} \ln \left[\frac{Z_{radar}}{\text{mm}^6 \text{ m}^{-3}} \right] \tag{5}$$

where Z_{radar} is the sum of the reflectivity calculated for each individual cloud particle category (e.g., cloud drops, raindrops, ice crystals, snow crystals, graupel and hail):

$$Z_{radar} = \left(\frac{6}{\pi \rho_w}\right)^2 \left[Z_c + Z_r + \frac{\rho_w^2}{\rho_i^2} \frac{|K_i^2|}{|K_w{}^2|} (Z_{ic} + Z_s + Z_g)\right]. \quad (6)$$

We added the description to Appendix A.

2. I also felt a lack of observational evidence of secondary ice production. The authors need to show observational data and explanations of the secondary ice production. Below are my comments.

   – For the case, both KDP and ZDR coincidentally increased at the same altitude. A signature of large KDP and large ZDR does not necessarily represent secondary ice production. Rather, it can be interpreted as size growth of individual particles (without secondary ice production). One of good signatures of secondary ice production is large KDP collocated with small ZDR. This can be seen Fig. S3, but less description about this in the text. In addition to such signature, the previous literature also showed other observational evidence such as in-situ data, Doppler spectra, and/or liquid water path. This manuscript did not show such evidence.

We thank the reviewer for the comment and the suggestion about the interpretation of the polarimetric signatures. We believe that this question arose because we did not provide the Hovmöller diagrams for K_{dp} and Z_{DR} between 13:00 and 17:30 UTC, but only for individual time steps (in Fig. 6 and Fig. S3). Now, we include Figure 2 which is the Hovmöller plots for K_{dp} and Z_{DR} between 13:00 and 17:30 UTC, as done previously for Z_{H} and the hydrometeor classification. It is more evident now, as the reviewer noticed for Fig. S3, that the peak of Z_{DR} is mostly below the peak of K_{dp}.

An interesting aspect of this case is that, while Z_{DR} reaches positive values that seldom exceed 1 dB (2dB as reference for the highest values), K_{dp} reaches values above 1.5 / 2 $^{\circ}\mathrm{km}^{-1}$ more frequently, which is instead extremely large for observations collected during a snow event. Because K_{dp} is affected by the number concentration while Z_{DR} is not, we interpreted this as a clear signature of a very large number concentration of hydrometeors from the perspective of the radar data. We can interpret these radar signatures as SIP when they are put into context of the model simulation that included collisional breakup as a SIP mechanism (e.g., BR28, BR2.8T and BR-Sot).

Regarding the latter part of the reviewer comment, we believe that we have multi-source complementary evidence: the radar signatures, 2DVD observations and model simulations. Unfortunately, Doppler spectra were not available at this time. As for the 2DVD, the number concentration was among the highest ever recorded at this location for this instrument during its deployment period (2009 to 2011). The largest 10-minutes average value of the number

concentration measured by the 2DVD during this case corresponds roughly to the 99.9% quantile of all the observations collected by this instrument at this location. In this specific case, the particles are also small as illustrated in Figure 1 of this document (on average around 0.5 mm with the 99% quantiles below 2 mm). We have, therefore, a very large number of small particles in the population of hydrometeors. Here, the model provides the required complementary evidence of SIP by the collisional breakup processes: only the model simulations with breakup produce the same order of magnitude in terms of number concentration, and they represent the Z_{H} profile better. We included the rime splintering simulation (RS) as our control simulation because the rime splintering process is traditionally used in numerical weather prediction models whereas collisional breakup is not. The RS simulation had very low to no SIP which resulted in less numerous but larger sized ice particles (Figs. 6a,b, 7f). These results do not agree with the 2DVD observations. In conclusion, we are confident that SIP occurred, not only from radar observations, but also by the concurrent information from the 2DVD and the collisional breakup simulations. The radar signatures, K_{dp} in particular, are so intense that they require in-depth investigation on the nature of the ice produced.

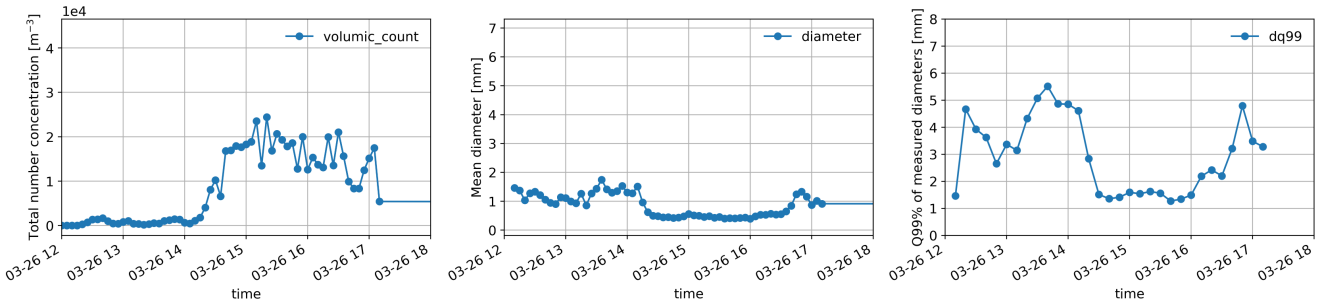

Figure 3. Evolution of (10-min) number concentration, mean diameter and quantile 99% of the diameters of the hydrometeors measured by the ground-based 2DVD.

In the revised manuscript we further stress the magnitude of the K_{dp} signature (Section *Case study*):

In particular K_{dp} reached values around 1.5 ° km^{-1} at certain height levels and towards the end of the event it was exceeding 2 ° km^{-1} (Fig. 2a). K_{dp} scales with radar frequency. A statistical analysis of K_{dp} in snowfall conducted with this radar and in this location but over a long observation period (Schneebeli et al., 2013), showed that the 80% quantile of K_{dp} at every height level is lower than 0.5 ° km^{-1}. Considering that the distribution of K_{dp} is very skewed, values above 1 ° km^{-1} in snow can be considered as unusually large.

In the Introduction we rephrased the explanation on the interpretation of K_{dp} and Z_{DR} with additional references to their interpretation in terms of SIP:

. . . specific differential phase shift K_{dp} [$^{\circ}\mathrm{km}^{-1}$]. This variable is complementary and not redundant: it is in fact not affected by the absolute calibration of a radar and is less affected than Z_{DR} by eventual presence of large isotropic particles within the sampling volume. Local K_{dp} enhancements in snowfall have been documented (Schneebeli et al., 2013; Bechini et al., 2013) and in some cases been associated with SIP (e.g., Andrić et al., 2013; Grazioli et al., 2015; Sinclair et al., 2016)

We clarified also how the 2DVD was used in this study when introducing the instruments in Sec. 2:

The 2DVD measures the size and fall velocity of hydrometeors larger than about 0.2 mm in terms of maximum dimension. The 2DVD is used in this study as ground reference to quantify the number concentration of snowfall particles (larger than 0.2 mm).

– Because of less figures from the observations (there are only reflectivity and hydrometeor classification plots), it was difficult to follow the first and second paragraphs of Sect. 3.1.1.

This is true, we should have made reference to figures 6(d, e) and S3(d, e). Additionally, we now show also K_{dp} and Z_{DR} in the new figure 3. We have adapted the manuscript to refer to the appropriate figures. The first reviewer, rightfully, also had difficulty with the second paragraph of 3.1.1. We modified the text to be more concise:

Z_{H} was significantly overestimated by the RS simulation between 13:00 and 17:30 UTC which most likely was a result of the following chain of events. 1) Insufficient droplets of size 25 µm (Fig. 5d), within the narrow temperature range ($-3 \geq T \geq -8\,^{\circ}$C), led to a limitation in ice particle growth by riming and therefore limited rime splintering (Fig. 6f). 2) Because rime splintering was not that active, typical for wintertime MPCs (e.g., Henneberg et al., 2017; Dedekind et al., 2021), the ice and snow crystals grew mainly by depositional growth and aggregation. 3) The ice and snow crystal size distributions widened substantially (Figs. 6a, b and S2a, b). These categories both had number concentrations less than 100 L^{-1} with particle diameters of up to 0.8 and 5.1 mm, respectively, at 15:30 UTC. 4) The larger ice and snow crystal diameters resulted in enhanced Z_{H}. These observation is consistent with other times during the day which showed even larger sized ice and snow crystals of 0.9 and 5.2 mm, respectively (Figs. S3a and S4a) as well as higher rain mass mixing ratios (e.g. Fig. 5a). There were single grid points where snow crystal even reached diameters of 13 to 17 mm during the latter part of the day (not shown here). Additionally, excessive size sorting in the model most likely contributed to the overestimation in Z_{H}. Size sorting typically occurs within the sedimentation parameterization of 2M schemes in regions of vertical wind shear or updraft cores (Milbrandt and McTaggart-Cowan, 2010; Kumjian and Ryzhkov, 2012). All these factors contributed to the RS simulation overestimating Z_{H} by at least 8 dBz throughout the vertical profile compared to the observations (Fig. 7d).

– RHI scans were performed from the low to high elevation angles (0-90 degrees). Observed Kdp and Zdr should have strong dependency on elevation angles. Did you correct the values for angles?

While other studies used some correction for elevation (notably Ryzhkov et al., 2005), for this study we decided instead not to use elevation angles above 40° (this was not mentioned in the original manuscript, so we thank the reviewer). It must be noted that, as RHIs are summarized with statistics along the $x-$ dimension, most of the data correspond to elevation angles well below 40° of elevation. The reason behind the choice not to correct for the polarimatric variables is that, at the time of this case study, the radar was not performing a regular bird-bath calibration of Z_{DR} and thus we cannot be confident that the accuracy of the differential reflectivity is around 0.1 dB or better, which is a prerequisite when applying the correction in a meaningful way (see Fig. 12 of Ryzhkov et al., 2005). This is now clarified in the text as:

Only observations obtained at elevation angles below 40° are used in order to limit the effect of elevation dependencies on the polarimetric variables (Ryzhkov et al., 2005).

– I was not sure how the 2DVD data were used other than number concentration. Did the 2DVD show good evidence of secondary ice production?

Please see our response to major point #1 above.

– Please explain how to estimate NICE and IWC from observation (e.g. Fig. 6, Fig. S3).

Following this comment and the suggestion of reviewer 1, we decided to include the full formulation of these retrievals as well as a thorough discussion of the inherent assumptions and shortcomings in Section 2.1. of the manuscript.

– Did you see shear instability?

Thanks for this question. We calculated the bulk Richardson which is a ratio of the buoyant energy to shear-kinetic energy. The Richardson number determines the dynamic stability of the air layer which becomes turbulent if the Richardson number is less than the critical Richardson number of 0.25. In Fig. 2 we show where the air layer was dynamically unstable, mainly as a result of the wind shear. It supports our conclusion that the wind shear enhanced the turbulence. In this case, the turbulence caused higher SIP rates through ice-graupel collisions. We also now mentioned this in the text in Section 3.1.

*Here, the bulk Richardson number, which is a ratio of the buoyant energy to shear-kinetic energy, is determined to asses the dynamic stability of the air layer. An air layer becomes turbulent if the Richardson number is less than the critical Richardson number of 0.25 (e.g., **?**). Figure 2b-e show where the air layer was turbulent which enhanced the interactions between ice particles and could have caused enhanced ice-graupel collisions. Regions of enhanced updraft, where hydrometeors can grow to larger sizes, were mostly seen immediately above the turbulent layer.*

Technical comments

1. Three digits are needed for latitude/longitude of the instrument locations.

   We thank the reviewer and we provide now the 3 digits for the 2DVD and MXPOL.

2. Line 123 “dual-Doppler radar output”: I was confused. Did you perform dual Doppler radar analysis (did you use two Doppler radars)? If so, please provide the second radar information.

   We thank the reviewer for spotting this confusion in the technical jargon. Indeed only one radar was used. We corrected the sentence to *dual-polarization*

3. Line 150: The use of consistent unit throughout the manuscript for temperature is better.

   We changed the temperature unit to °C.

4. 3.2: What criteria were used for separating the period?

   The three periods were seperated by the location and intensity of the wind shear and corresponding turbulent layer.

   13:00-14:15: Strong wind shear and turbulence mixing at lower altitudes below 3 km with a stronger updraft regions above the turbulent layer. Graupel beginning to form and grow in size.

   14:30-15:45: The turbulent layer ascends to 4 km and into temperature region where SIP from collisional breakup is more favored.

   16:00-17:15: The wind shear reduces substantially causing the turbulent layer to dissipate. The updraft in this period is reduced and the cloud is in a glaciated state which should not favor SIP.

   We added the following description to Section 3.3:

   The early period was categorized with strong wind shear and a turbulent layer below 3 km (Fig. 2b-e). During the middle period the turbulent layer extended to 4 km during which graupel was becoming more dominant in the MPC. The late period was categorized by less wind shear causing the dissipation of the turbulent layer. The cloud entered a glaciated state during this time.

References

Andrić, J., Kumjian, M. R., Zrnić, D. S., Straka, J. M., and Melnikov, V. M.: Polarimetric Signatures above the Melting Layer in Winter Storms: An Observational and Modeling Study, Journal of Applied Meteorology and Climatology, 52, 682–700, https://doi.org/10.1175/JAMC-D-12-028.1, publisher: American Meteorological Society Section: Journal of Applied Meteorology and Climatology, 2013.

Bechini, R., Baldini, L., and Chandrasekar, V.: Polarimetric Radar Observations in the Ice Region of Precipitating Clouds at C-Band and X-Band Radar Frequencies, Journal of Applied Meteorology and Climatology, 52, 1147–1169, https://doi.org/10.1175/JAMC-D-12-055.1, publisher: American Meteorological Society Section: Journal of Applied Meteorology and Climatology, 2013.

Dedekind, Z., Lauber, A., Ferrachat, S., and Lohmann, U.: Sensitivity of precipitation formation to secondary ice production in winter orographic mixed-phase clouds, Atmospheric Chemistry and Physics, 21, 15 115–15 134, https://doi.org/10.5194/acp-21-15115-2021, 2021.

Grazioli, J., Lloyd, G., Panziera, L., Hoyle, C. R., Connolly, P. J., Henneberger, J., and Berne, A.: Polarimetric radar and in situ observations of riming and snowfall microphysics during CLACE 2014, Atmospheric Chemistry and Physics, 15, 13 787–13 802, https://doi.org/10.5194/acp-15-13787-2015, 2015.

Henneberg, O., Henneberger, J., and Lohmann, U.: Formation and Development of Orographic Mixed-Phase Clouds, Journal of the Atmospheric Sciences, 74, 3703–3724, https://doi.org/10.1175/JAS-D-16-0348.1, 2017.

Kumjian, M. R. and Ryzhkov, A. V.: The Impact of Size Sorting on the Polarimetric Radar Variables, Journal of the Atmospheric Sciences, 69, 2042–2060, https://doi.org/10.1175/JAS-D-11-0125.1, publisher: American Meteorological Society Section: Journal of the Atmospheric Sciences, 2012.

Milbrandt, J. A. and McTaggart-Cowan, R.: Sedimentation-Induced Errors in Bulk Microphysics Schemes, Journal of the Atmospheric Sciences, 67, 3931–3948, https://doi.org/10.1175/2010JAS3541.1, 2010.

Ryzhkov, A. V., Giangrande, S. E., Melnikov, V. M., and Schuur, T. J.: Calibration Issues of Dual-Polarization Radar Measurements, Journal of Atmospheric and Oceanic Technology, 22, 1138–1155, https://doi.org/10.1175/JTECH1772.1, publisher: American Meteorological Society Section: Journal of Atmospheric and Oceanic Technology, 2005.

Schneebeli, M., Dawes, N., Lehning, M., and Berne, A.: High-Resolution Vertical Profiles of X-Band Polarimetric Radar Observables during Snowfall in the Swiss Alps, Journal of Applied Meteorology and Climatology, 52, 378–394, https://doi.org/10.1175/JAMC-D-12-015.1, 2013.

Seifert, A.: Parametrisierung wolkenmikrophysikalischer Prozesse und Simulation konvektiver Mischwolken, Doctoral Thesis, Universitat Karlsruhe, Forschungszentrum Karlsruhe, https://www.imk-tro.kit.edu/4437_1388.php, 2002.

Sinclair, V. A., Moisseev, D., and von Lerber, A.: How dual-polarization radar observations can be used to verify model representation of secondary ice, Journal of Geophysical Research: Atmospheres, 121, 10,954–10,970, https://doi.org/10.1002/2016JD025381, _eprint: https://onlinelibrary.wiley.com/doi/pdf/10.1002/2016JD025381, 2016.

Sotiropoulou, G., Vignon, , Young, G., Morrison, H., O'Shea, S. J., Lachlan-Cope, T., Berne, A., and Nenes, A.: Secondary ice production in summer clouds over the Antarctic coast: an underappreciated process in atmospheric models, Atmospheric Chemistry and Physics, 21, 755–771, https://doi.org/10.5194/acp-21-755-2021, 2021.

Sullivan, S. C., Barthlott, C., Crosier, J., Zhukov, I., Nenes, A., and Hoose, C.: The effect of secondary ice production parameterization on the simulation of a cold frontal rainband, Atmospheric Chemistry and Physics, 18, 16 461–16 480, https://doi.org/10.5194/acp-18-16461-2018, 2018.

Takahashi, T., Nagao, Y., and Kushiyama, Y.: Possible High Ice Particle Production during Graupel–Graupel Collisions, Journal of the Atmospheric Sciences, 52, 4523–4527, https://doi.org/10.1175/1520-0469(1995)052<4523:PHIPPD>2.0.CO;2, 1995.